

Charged nanoparticles as supramolecular surfactants for controlling the growth and stability of microcrystals

Bartłomiej Kowalczyk^{1,2}, Kyle J. M. Bishop³, Istvan Lagzi^{1,2}, Dawei Wang¹, Yanhu Wei^{1,2}, Shuangbing Han^{1,2} and Bartosz A. Grzybowski^{1,2}*

Microcrystals of desired sizes are important in a range of processes and materials, including controlled drug release^{1,2}, production of pharmaceuticals and food^{3,4}, bio-⁵ and photocatalysis⁶, thin-film solar cells⁷ and antibacterial fabrics⁸. The growth of microcrystals can be controlled by a variety of agents, such as multivalent ions⁹, charged small molecules¹⁰, mixed cationic-anionic surfactants^{11,12}, polyelectrolytes^{13,14} and other polymers¹⁵, micropatterned self-assembled monolayers^{16,17}, proteins¹⁸ and also biological organisms during biomineralization^{19,20}. However, the chief limitation of current approaches is that the growth-modifying agents are typically specific to the crystallizing material. Here, we show that oppositely charged nanoparticles can function as universal surfactants that control the growth and stability of microcrystals of monovalent or multivalent inorganic salts, and of charged organic molecules. We also show that the solubility of the microcrystals can be further tuned by varying the thickness of the nanoparticle surfactant layers and by reinforcing these layers with dithiol crosslinks.

In the method we describe, the formation of nanoparticle (NP)-protected microcrystals results from an interplay between crystal growth, polyvalent crystal–NP interactions and the NP–NP interactions that mediate the particles' cooperative adsorption onto the growing crystals. Depending on the relative concentrations of the NPs and the co-crystallizing salts, it is possible to adjust the sizes of the microcrystals (from several micrometres to ~100 nm) and also the thickness of the NP layers coating them (from NP monolayers to multilayers). Remarkably, these protective NP coatings can also act to stabilize the crystals so as to modulate their solubility, which can have implications for controlled-release applications^{21,22}.

Most experiments were based on inorganic salts—including those of monovalent (K₂SO₄, Na₂SO₄) and bivalent (CaCO₃, Cu(OH)₂) cations—although the method was equally applicable to charged organic molecules such as L-lysine or vitamin B₅ (Fig. 1). When crystallized from water–dimethyl sulphoxide mixtures, these salts and compounds grew large crystals, typically hundreds of micrometres across and, irrespective of the experimental conditions tested (dilution, temperature), not smaller than several tens of micrometres. Crystal sizes decreased markedly—to a few micrometres or even tens of nanometres—when the salts were crystallized in the presence of charged, ~5.5 ± 0.6 nm gold and/or silver NPs. Half of the NPs were coated with positively charged *N,N,N*-trimethyl

(11-mercaptoundecyl)ammonium chloride (TMA) thiols and half with deprotonated, negatively charged 11-mercaptoundecanoic acid (MUA) thiols (at pH 11, adjusted with tetramethylammonium hydroxide; for preparation, see refs 23–25 and Methods). In a typical crystallization procedure, NPs and a desired inorganic salt were dissolved in a mixture of deionized water and dimethyl sulphoxide. This mixture was heated at $T = 65\text{ }^{\circ}\text{C}$ to evaporate water (the 'good solvent') over the course of one to two days (for details, see Methods). Towards the end of water evaporation, the solution's colour (due to the free NPs) gradually faded as the microcrystals and NPs precipitated as a fine powder. The microcrystals thus grown were then imaged by scanning electron microscopy (SEM, on a Leo 1525 system) and transmission electron microscopy (TEM, on a Hitachi 8100), which revealed NPs adsorbed onto the crystals' surface. Despite their presence, the crystal habits were the same as those of crystals grown without NPs, suggesting that particles adsorb non-specifically onto the various crystal facets (that is, they do not act as structure-directing surfactants). In addition, the composition of the microcrystals was examined using scanning TEM (Hitachi 2300) or high-resolution TEM (Jeol) equipped with an electron dispersive X-ray spectroscopy detector. These scans confirmed the presence of NPs on the crystals. Of particular importance were the experiments using oppositely charged NPs with different metal cores (for example, AgTMA and AuMUA)—in this case, electron dispersive X-ray spectroscopy spectra revealed that both the Ag(+) and Au(–) adsorbed onto the microcrystals (Fig. 1c). Also, it is worth noting that the powder X-ray diffraction spectra of crystals covered and not covered with the NPs (Fig. 1d) were similar, indicating that adsorption of the NPs did not alter the crystal structure.

The key parameter controlling the outcome of crystallizations is the ratio of the concentration of the NPs to the concentration of the salt, $\chi = C_{\text{NP}}/C_{\text{salt}}$. When χ is large ($> \sim 5$) and the NPs are present in excess, electrostatic interactions between the NPs dominate and mediate self-assembly of all-nanoparticle crystals (Fig. 2a) as described in detail in refs 25,26. Conversely, when χ is small ($< \sim 0.2$), the NPs flocculate into orderless aggregates, probably owing to the bridging of nanoparticles through chelating interactions^{27,28} (Fig. 2d). The optimal range for the controlled growth of the microcrystals is $0.25 < \chi < 4.0$ (Fig. 2c). In this regime, the majority of the available NPs form 1-NP-thick 'skins' around the salt microcrystals, with no uncoated salt crystals being present. High-resolution SEM images show that the NP

¹Department of Chemical and Biological Engineering, Northwestern University, 2145 Sheridan Rd., Evanston, Illinois 60208, USA, ²Department of Chemistry, Northwestern University, 2145 Sheridan Rd., Evanston, Illinois 60208, USA, ³Department of Chemical Engineering, The Pennsylvania State University, University Park, Pennsylvania 16802, USA. *e-mail: grzyb@northwestern.edu.

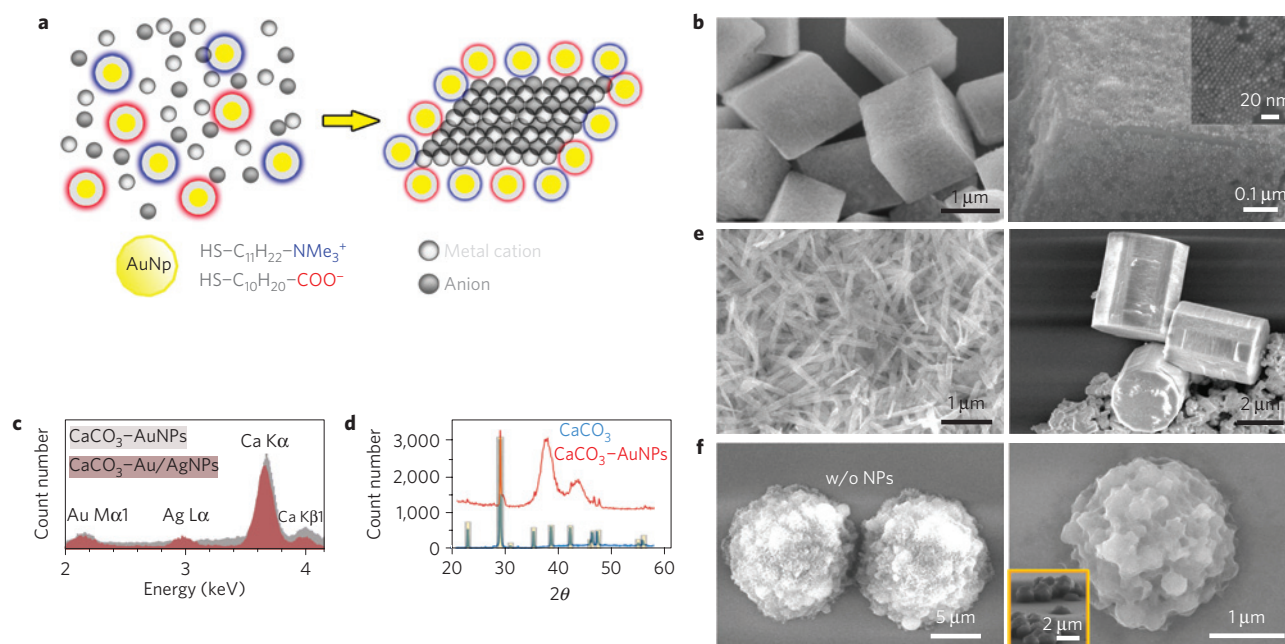


Figure 1 | NP surfactants control the growth of inorganic salt microcrystals. **a**, Schematic representation of the process of crystal growth. When the salt starts to crystallize, NPs adsorb onto the crystal's faces, thereby slowing its growth. **b**, SEM images—at two different magnifications—of calcite microcrystals coated with NP monolayers. The right-hand image illustrates that the NP coating is sparser near the microcrystal's edges. Inset: Magnified view of the regularly packed domains within the NP monolayer. **c**, Two overlaid compositional electron dispersive X-ray spectroscopy scans of calcite crystals coated with a monolayer of Au(+)/Au(−) NPs (grey) and Ag(+)/Au(−) NPs (brown). In both cases, the peaks characteristic of gold are visible; the silver peak, however, is present only for the crystals covered with Ag(+)/Au(−) NPs. **d**, Powder X-ray diffraction spectra of calcite crystals grown with and without AuNP coatings. For X-ray diffraction spectra comparing large and small crystals see Supplementary Fig. S6. **e**, Two further examples of NP-coated microcrystals: left, $\text{Cu}(\text{OH})_2$; right, K_2SO_4 . More examples are included in Supplementary Figs S3 and S4. **f**, SEM images of L-lysine microcrystals grown in the absence (left) and in the presence (right) of Au NPs ($C_{\text{NP}} = 0.8 \text{ mM}$, $C_{\text{lysine}} = 3 \text{ mM}$). Close-ups of the NP-covered crystal faces are included in Supplementary Section S1.

coatings consist of domains of relatively regular NP packing, and are typically denser in the middle of the crystal faces than near their edges (Supplementary Section S1). Importantly, as χ increases, the size of the microcrystals, d , decreases from several micrometres all the way to hundreds of nanometres (Fig. 3c); this decrease is well approximated as $d \sim 1/\chi$ (dashed line in Fig. 3c). Such a scaling might indeed be expected because the number of ions forming a microcrystal of size d scales as d^3 , whereas the number of NPs necessary to build a protective 'skin' around it scales as d^2 .

An important observation to make is that controlled microcrystal growth requires the presence of both positively and negatively charged NPs. With particles of only one polarity present in the solution, the electrostatic repulsions between these NPs limit their deposition onto the crystals, which then grow unhindered to large dimensions. In sharp contrast, when positive and negatively charged NPs are present, they can adsorb cooperatively²⁹. Each adsorbed NP not only interacts with the crystal (through electrostatic^{30,31}, van der Waals and chelating²⁸ interactions^{30,31}; see Supplementary Section S3 for the discussion of forces acting in the system) but also facilitates the attachment of a neighbouring particle of opposite polarity. The adsorption process continues until the NPs deposit an electroneutral coating, in which the overall compensation of NP charges ($\sum Q_{\text{NP}(+)} + \sum Q_{\text{NP}(-)} = 0$) limits adsorption of further nanoparticles. When the AuMUA particles are fully deprotonated (as at pH 11), electroneutrality is achieved on formation of a NP monolayer (for details of this mechanism, see refs 29 and 31).

We emphasize that the immobilization of MUA and TMA ligands onto NPs is essential for the coating process. When these molecules are unattached and free in solution, they are

not capable of regulating the growth of the crystals we studied. This observation suggests a crucial role of polyvalent interactions acting in the system. Because adsorption from a dilute solution onto a surface is entropically unfavourable (with penalty $\Delta S \sim k_{\text{B}}T \ln(Ad/V)$ for the translational degrees of freedom of each adsorbed species; $k_{\text{B}}T$ is the thermal energy, A is the total area available to the adsorbate, d is the size of the adsorbate and V is the solution volume), the interactions between the adsorbate and the crystal surface must be sufficiently strong to yield an overall favourable (negative) free energy of adsorption. For small-molecule growth inhibitors, strong binding requires rather precise molecular recognition of a particular crystal surface (for example, phosphonates on BaSO_4 ; ref. 32); consequently, these inhibitors are not universally effective. Similar binding affinities can also be achieved through many non-specific interactions acting in concert. Such polyvalent interactions provide a basis for versatile NP surfactants that adsorb strongly to a variety of different surfaces. In addition to polyvalent interactions between charged ligands bound to the NPs and the crystal surface, the charged nanoparticles described here benefit further from the (+)/(−) interparticle interactions, which facilitate their non-specific adsorption to a variety of surfaces.

Mechanistically, a plausible scenario of the crystallization–deposition process is that the NPs adsorb non-specifically onto the surfaces of the growing crystals to physically retard their growth. In this process, the kinetics of crystal growth competes with that of NP monolayer formation²⁹. As NPs gradually adsorb in time onto the crystal surface, the rate of crystal growth decreases—consequently, an increase in NP concentration results in faster NP adsorption, slower crystal growth, and thereby smaller crystals on formation of a complete NP monolayer.

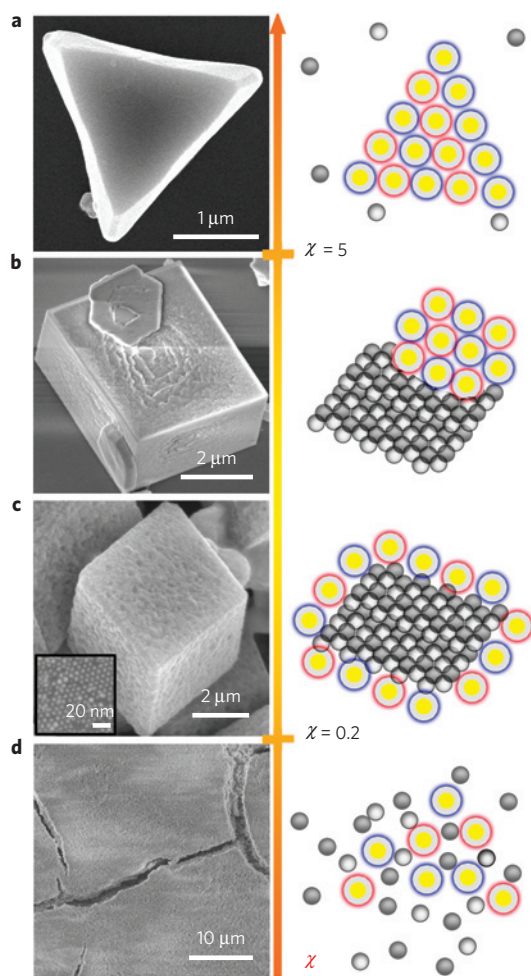


Figure 2 | The nature of the assembling structures depends on the ratio of NP and salt concentrations, $\chi = C_{\text{NP}}/C_{\text{salt}}$.

The SEM images in the left-hand column and the schematic representations in the right-hand column illustrate qualitatively different χ regimes observed in experiments with all salts tested; the actual scanning electron micrographs shown are for the case of CaCO_3 at $\text{pH} \sim 11$ (fully deprotonated MUA AuNPs).

a, When $\chi \gg 5$, the NPs assemble into micrometre-sized, all-NP crystals; the remaining salt remains in solution. **b**, When χ is lowered toward ~ 4 , the all-NP crystals are still present but are attached to salt microcrystals, usually in the middle of the microcrystals' faces. In this regime, however, the sizes of the microcrystals cannot be precisely controlled.

c, For $4 > \chi > 0.25$, the NPs form monolayers on the crystals. Formation of these monolayers competes with crystal growth (main text) and effectively controls the size of the microcrystals. **d**, Finally, when χ is small ($< \sim 0.2$) NPs precipitate into orderless aggregates whereas excess salt remains in solution.

Interestingly, by making the reasonable assumptions that NP adsorption onto the microcrystals is described by a Langmuir-type kinetic model and the rate of crystal growth is proportional to the free crystal surface area, the proposed mechanism reproduces the experimentally observed scaling of the crystal size, $d \sim 1/\chi$ (Fig. 3c), and also agrees with the time-course data in Fig. 3a,b, where the crystals are seen to grow only to a certain size (for further model details, see Supplementary Section S2). We note that an alternative scenario, in which the NPs would nucleate the growth of the microcrystals, seems unlikely—assuming the number of nucleated crystals scales with the number of NPs, we would then expect the scaling $d \sim (1/\chi)^{1/3}$, which is not observed experimentally.

A corollary to the proposed mechanism is that the NP/microcrystal structures should not form if the solubility of the salt is higher than that of the NPs—under these conditions, NPs are expected to crystallize or aggregate before the formation of any microcrystals onto which the NPs might otherwise adsorb. This was indeed verified in a set of experiments with highly soluble salts, including NaCl (solubility product, $K_{\text{SP}} \sim 36 \text{ M}^2$), KCl ($K_{\text{SP}} \sim 23 \text{ M}^2$) and CaCl_2 ($K_{\text{SP}} \sim 1,209 \text{ M}^3$). When these salts were present in high concentrations, they facilitated ion-bridging interactions between the NPs (refs 27,28), causing them to precipitate from solution as orderless aggregates before any salt crystals formed. Likewise, when the salt concentration was low, NPs formed all-nanoparticle crystals whereas the salt remained dissolved.

In addition to the ratio of the NP and salt concentrations, the structures of the NP/microcrystal composites can be controlled by the pH. Specifically, as the pH is lowered (from 11.0 to ~ 6.5 ; below the latter value NPs precipitate) and MUA ligands become partly protonated, the thickness of the NP coatings on the crystals gradually increases (probably owing to hydrogen bonding between MUA NPs; ref. 31). At around $\text{pH} = 9.0$, the coatings are a few NP layers thick, whereas at $\text{pH} \sim 8.5$ their thickness becomes commensurate with the dimensions of the microcrystals themselves and they form large parallelepipeds, often with sharp, well-defined edges. A striking manifestation of this behaviour is illustrated in Fig. 4a, where the NPs deposit on a CaCO_3 crystal to form a cross-like composite structure. In this and other systems at lowered pH, deposition of multilayers can be attributed to the protonation of the carboxylic acids on the MUA NPs. Whereas this protonation weakens the electrostatic interactions between the NPs, it also enables the MUA particles to engage in hydrogen bonding such that they become more 'sticky' with respect to one another³¹.

Finally, once formed, both the NP monolayers and multilayers on the microcrystals can be further stabilized by crosslinking the proximal NPs with alkane dithiols (typically, 0.1 M in acetonitrile; Fig. 4b and ref. 33). Importantly, this 'reinforcement' allows for control of the solubility of the microcrystals. This is illustrated in Fig. 4c, which quantifies (by means of inductively coupled plasma atomic emission spectroscopy, ICP AES, see Methods) the amounts of calcium dissolved from CaCO_3 μC 's stabilized with crosslinked NP layers of different thicknesses, H , and immersed in 0.1 mM HCl. As plotted in Fig. 4d, the rates of crystal dissolution, k , decrease with increasing H , and change by a factor of five to six between uncoated microcrystals and those coated with ~ 50 nm NP layers. We note that this k versus H trend is in line with the predictions of a theoretical model of crystal dissolution described in detail in Supplementary Section S4; the dashed line in Fig. 4d gives the theoretical fit to the experimental data.

In summary, we demonstrated that the growth and the stability of various microcrystals can be controlled by charged NP surfactants. Of particular promise is the ability to control the solubility of the microcrystals, which can have implications for controlled-delivery applications. One obvious challenge for future research is to extend the present methodology to systems in which the NPs would control crystal habits (this would probably require design of NPs that interact differently with different types of crystal face). The use of NP interactions other than electrostatic should also be considered, especially in designing NP surfactants for crystals of organic molecules.

Methods

Synthesis and functionalization of AuNPs. AuDDA NPs. Dodecylamine (DDA)-coated gold NPs were prepared according to a modified literature procedure^{24,25}. Here, we used $\text{HAuCl}_4 \cdot 3\text{H}_2\text{O}$ instead of AuCl_3 and obtained AuDDA NPs of average sizes (d) = 5.5 nm and size dispersity $\sim 11\%$. The average sizes of the particles were estimated on the basis of TEM images of at least 500 NPs from each batch used.

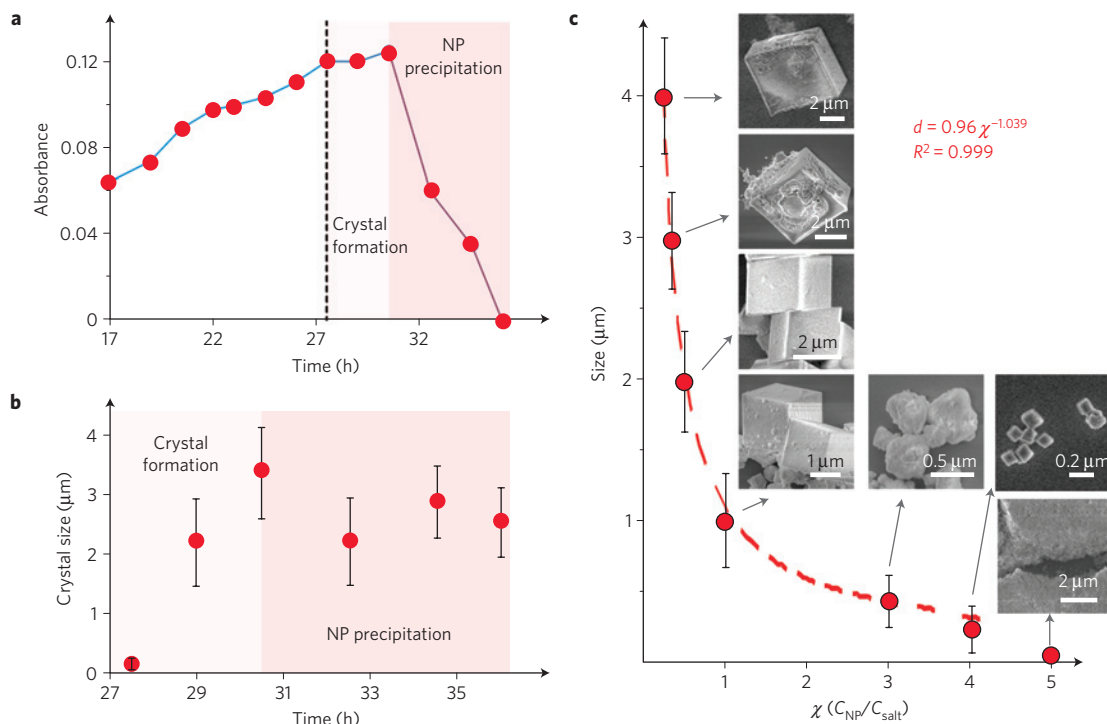


Figure 3 | Time course of crystallization and crystal-size control. **a,b**, A typical time course of the crystallization process in which $C_{\text{salt}} = 0.67$ mM of CaCO_3 was crystallized in the presence of $C_{\text{NP}} = 0.27$ mM AuMUA/AuTMA NP mixture. At each time, an aliquot of solution was taken and centrifuged: the supernatant solution was analysed by ultraviolet–visible spectroscopy, and the sediment (if any) was imaged by SEM. **a**, The solution’s absorbance at 520 nm, corresponding to the surface plasmon resonance maximum of the AuNPs. Initially, the absorbance increases, reflecting evaporation of water and the solution becoming more concentrated. In this regime, no crystals are seen in the corresponding scanning electron micrographs. Crystallization commences at about 29 h and is accompanied by a decrease in the surface plasmon resonance intensity due to NPs coating the forming microcrystals and also precipitating from solution (as seen in the scanning electron micrographs as ‘free’ NPs not on the microcrystals). The crystal size is approximately $2.5 \mu\text{m}$, consistent with the data shown in **c**. The data shown in **a** and **b** are based on the analysis of 16 independent crystallization experiments; for SEM analyses, at least ten crystals from each experiment were imaged for each time point. The error bars in **b** represent 1 s.d. above and below the mean obtained from a sample of at least 20 crystals. **c**, Control of crystal size. As the concentration of the NPs, C_{NP} , increases (for a given C_{salt}), the size of the microcrystals decreases. The images here are for microcrystals of calcium carbonate at pH 11 and $C_{\text{salt}} = 1$ mM. Insets show typical crystals. S.d. of crystal size is based on at least 50 microcrystals from three separate batches (for further images, see Supplementary Fig. S5). The dashed line is the best fit to the $\chi \propto 1/d$ dependence (d being the characteristic crystal size).

Ligand exchange on gold NPs. All ultrapure-grade thiols (MUA and TMA) were obtained from ProChimia Surfaces (www.prochimia.com) and used as received. A toluene solution of DDA-capped AuNPs ($7 \mu\text{mol ml}^{-1}$, 20 ml, 140 μmol) was quenched with 100 ml of methanol to give a black precipitate. The supernatant solution with excess of capping agent and surfactant was decanted, and the precipitate was washed with methanol (50 ml) and dissolved in toluene (100 ml), to which a thiol solution (140 μmol) in 10 ml of CH_2Cl_2 was added on stirring. The precipitate of thiol-coated AuNPs was left to settle down, the mother liquor solution was decanted, and the solid was washed with CH_2Cl_2 (3×30 ml). The precipitate was then dissolved in 5 ml of methanol on sonication. The AuMUA were deprotonated with 25% methanolic solution of NMe_4OH (70 μl , 165 μmol), precipitated with acetone (30 ml) and washed with acetone (2×30 ml). The AuTMAs were precipitated with ethyl acetate (100 ml) and washed with CH_2Cl_2 and acetone. Finally, all the precipitates of thiol-coated AuNPs were dried and dissolved in 13 ml of water to obtain ~ 10 mM (in terms of numbers of metal atoms) NP solutions. In the case of AuMUA the pH of the solution was adjusted to ~ 11 with 0.2 M solution of NMe_4OH .

Preparation of a mixture of oppositely charged nanoparticles. Electroneutral (in terms of charges on the NPs) solutions of TMA-coated NPs and deprotonated (at pH 11) MUA-coated NPs were obtained by titrating the NPs of one polarity with the solution of NPs of the oppositely polarity. In a typical procedure, AuMUA solution (10 ml of 2.0 mM, 20 μmol in terms of metal atoms) was titrated with aliquots of 2.0 mM AuTMA solution under vigorous stirring. The NP mixture was stable during the titration but precipitated sharply at the point of electroneutrality, when the total negative charge on MUA NPs was balanced by the total positive charge of the TMA nanoparticles. Precipitated NPs were collected, centrifuged and washed with DI water to remove excess salts. Finally, NPs were redissolved in DI water on gentle heating. This solution was then stable for several months. For further details, see refs 23–26.

General procedure for crystallization of salts in the presence of NPs. Aqueous solution of salt (2 ml, $C_{\text{salt}} \sim 0.15$ – 3.0 mM) was placed in a glass vial and mixed with 3–60 μl of $C_{\text{NP}} = 50$ mM (in terms of metal atoms) solution of oppositely charged NPs. The pH of the salt-NP solution was adjusted to a desired value by the addition of tetramethylammonium hydroxide (TMAOH). To this mixture, 1 ml of dimethyl sulphoxide was added (so that $C_{\text{NP}} \sim 0.1$ – 2.0 mM and $C_{\text{salt}} \sim 0.1$ – 2.0 mM in ~ 3 ml total volume). The mixture was heated at $T = 65^\circ\text{C}$ to evaporate water (the ‘good solvent’) over the course of 1–2 days. Notes: Copper hydroxide crystals were grown from copper sulphate ($\text{Cu}^{2+} + 2\text{OH}^- \rightarrow \text{Cu}(\text{OH})_2$ at pH = 11, adjusted by addition of TMAOH). Calcium carbonate crystals were grown from the calcium hydroxide precursor solution (freshly prepared by reacting CaO with water to yield a solution of calcium hydroxide, $C_{\text{salt}} \sim 0.15$ – 3.0 mM, in the following reaction: $\text{Ca}(\text{OH})_2 + \text{CO}_2 \rightarrow \text{CaCO}_3 + \text{H}_2\text{O}$). The pH of as-prepared solution was ~ 10 – 11 and after mixing with NP solution it was adjusted to 11 (or 8–11 as in the experiments in Fig. 4a) by addition of TMAOH or HCl. Lysine crystals were grown from L-lysine solutions at the concentrations $C_{\text{lysine}} \sim 1$ – 6 mM and pH ~ 11 (adjusted by addition of TMAOH). Potassium and sodium sulphate crystals were grown at pH ~ 11 . Magnesium sulphate crystals were grown at pH ~ 8 to avoid formation of $\text{Mg}(\text{OH})_2$ ($\text{Mg}^{2+} + 2\text{OH}^- \rightarrow \text{Mg}(\text{OH})_2$).

Kinetics of crystal dissolution studied by ICP AES. Calcite crystals (containing 1 μmol of calcium) without NP coating and coated with NP layers of different thicknesses were placed into 10 ml of 0.1 mM HCl solution at pH = 4. Small (300 μl) aliquots of the supernatant were drawn carefully at predetermined time intervals, and were diluted with 3% nitric acid up to 3 ml. These solutions were analysed by ICP AES (on a Varian Vista MPX instrument), and the amounts of Ca^{2+} were determined from the intensity of the Ca^{2+} peak at wavelength 396.847 nm. Together, these measured amounts gave the dissolution kinetics curves in Fig. 4c.

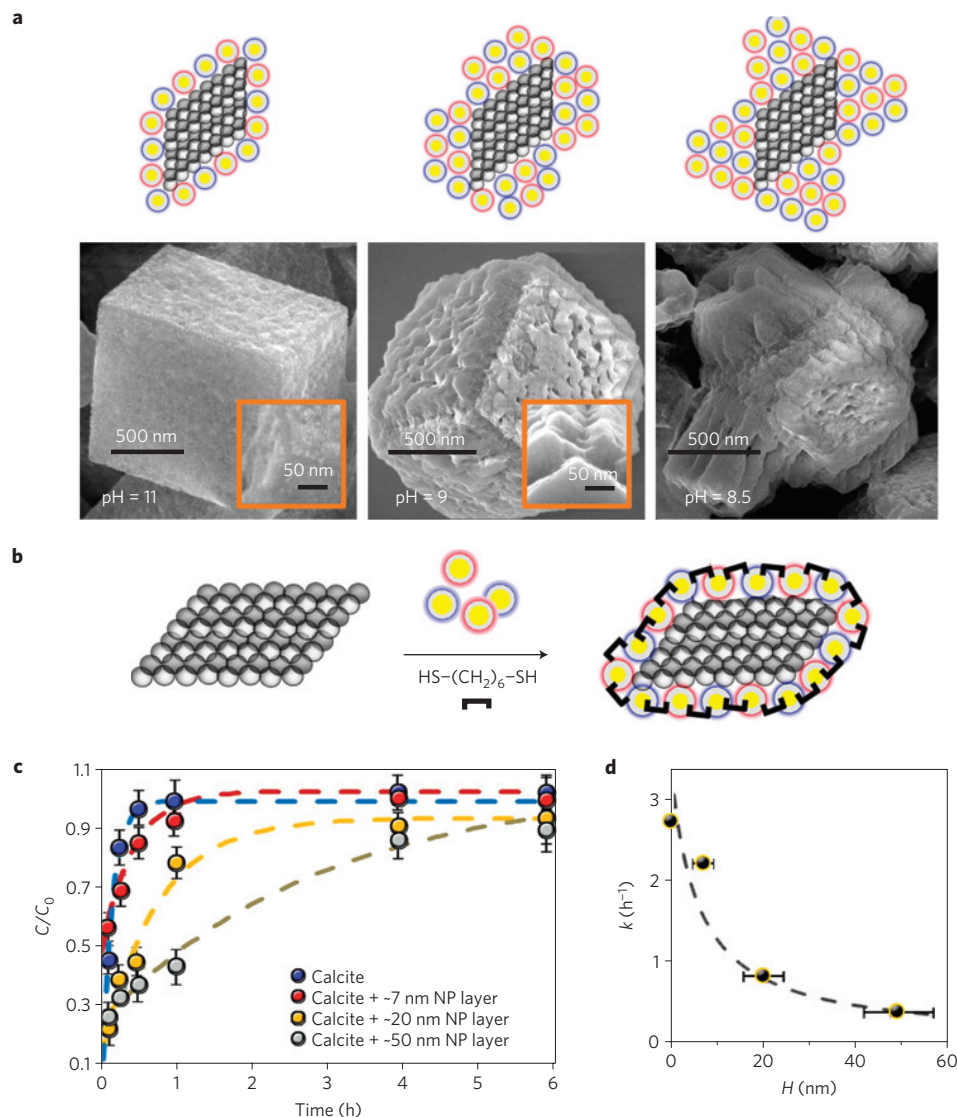


Figure 4 | Varying the thickness of the NP shell and controlling the microcrystals' solubility. **a**, When the pH is lowered and the MUA NPs become partly protonated, the thickness of the NP layers coating the microcrystals increases from 5–6 nm (monolayer) at pH 11, to ~50-nm-thick multilayers at pH 9, to pyramid-like formations protruding from the microcrystals' faces at pH 8.5. The SEM images shown here are for calcite crystals. The magnified insets show the vertices of the crystals and illustrate that the NP coatings therein are sparse or even absent (Fig. 1b, right image; Supplementary Section S2).

b, Schematic representation of experiments, in which the proximal NPs coating the microcrystals are crosslinked with alkane dithiols (for example 1,6-hexanedithiol). **c**, Crosslinking reduces crystal solubility. The graph plots, as a function of time, the concentrations of Ca^{2+} liberated from the uncoated (blue circles) calcite crystals, and from calcite crystals coated with crosslinked NP layers of different thicknesses, H . In all cases, the crystals were immersed in a 0.1 mM aqueous solution of HCl (pH 4). The amounts of Ca^{2+} released were measured by ICP AES (Methods). Error bars correspond to three independent sets of experiments for each type of crystal. Dashed lines are fits to the first-order dissolution kinetics (for details of the model, see Supplementary Section S4). **d**, The circles give the experimental dissolution rate constants based on the fits in **c**. The dashed line is the prediction of the theoretical model (Supplementary Section S4). The horizontal error bars in this plot give the s.d. in the NP layer thickness, H (as determined by high-resolution SEM imaging of at least 20 crystals for each sample).

Received 11 April 2011; accepted 16 November 2011;
published online 10 January 2012; corrected online
20 January 2012

References

1. Ai, H., Jones, S. A., de Villiers, M. M. & Lvov, Y. M. Nano-encapsulation of furosemide microcrystals for controlled drug release. *J. Control. Release* **86**, 59–68 (2003).
2. Qiu, X. P., Leporatti, S., Donath, E. & Mohwald, H. Studies on the drug release properties of polysaccharide multilayers encapsulated ibuprofen microparticles. *Langmuir* **17**, 5375–5380 (2001).
3. Ek, R., Wormald, P., Ostelius, J., Iversen, T. & Nyström, C. Crystallinity index of microcrystalline cellulose particles compressed into tablets. *Int. J. Pharm.* **125**, 257–264 (1995).
4. Bodmeier, R. Tableting of coated pellets. *Eur. J. Pharm. Biopharm.* **43**, 1–8 (1997).
5. Kreiner, M., Moore, B. D. & Parker, M. C. Enzyme-coated micro-crystals: A 1-step method for high activity biocatalyst preparation. *Chem. Commun.* **41**, 1096–1097 (2001).
6. Pradhan, A. R., Macnaughtan, M. A. & Raftery, D. Zeolite-coated optical microfibers for intrazeolite photocatalysis studied by *in situ* solid-state NMR. *J. Am. Chem. Soc.* **122**, 404–405 (2000).
7. Rech, B. *et al.* Microcrystalline silicon for large area thin film solar cells. *Thin Solid Films* **427**, 157–165 (2003).
8. Lee, G. S., Lee, Y. J., Ha, K. & Yoon, K. B. Preparation of flexible zeolite-tethering vegetable fibers. *Adv. Mater.* **13**, 1491–1495 (2001).
9. Kubota, N., Otosaka, H., Doki, N., Yokota, M. & Sato, A. Effect of lead(II) impurity on the growth of sodium chloride crystals. *J. Cryst. Growth* **220**, 135–139 (2000).

- Mann, S., Didymus, J. M., Sanderson, N. P., Heywood, B. R. & Samper, E. J. A. Morphological influence of functionalized and non-functionalized- α , ω -dicarboxylates on calcite crystallization. *J. Chem. Soc. Faraday Trans.* **86**, 1873–1880 (1990).
- Jing, S. Y. *et al.* Synthesis of octahedral Cu₂O microcrystals assisted with mixed cationic/anionic surfactants. *Mater. Lett.* **61**, 2281–2283 (2007).
- Tian, G. R., Sun, S. X., Song, X. Y., Zhao, W. & You, T. Cooperative role of dual surfactants in synthesis of single crystal BaMoO₄ microcrystals. *Mater. Technol.* **24**, 92–96 (2009).
- Xiao, J. J., Kan, A. T. & Tomson, M. B. Prediction of BaSO₄ precipitation in the presence and absence of a polymeric inhibitor: Phosphino-polycarboxylic acid. *Langmuir* **17**, 4668–4673 (2001).
- Oner, M. & Akyol, E. Inhibition of calcium oxalate monohydrate crystal growth using polyelectrolytes. *J. Cryst. Growth* **307**, 137–144 (2007).
- Yang, J. H., Qi, L. M., Zhang, D. B., Ma, J. M. & Cheng, H. M. Dextran-controlled crystallization of silver microcrystals with novel morphologies. *Cryst. Growth Des.* **4**, 1371–1375 (2004).
- Aizenberg, J., Black, A. J. & Whitesides, G. H. Oriented growth of calcite controlled by self-assembled monolayers of functionalized alkanethiols supported on gold and silver. *J. Am. Chem. Soc.* **121**, 4500–4509 (1999).
- Aizenberg, J., Black, A. J. & Whitesides, G. M. Control of crystal nucleation by patterned self-assembled monolayers. *Nature* **398**, 495–498 (1999).
- Yeh, Y. & Feeney, R. E. Antifreeze proteins: Structures and mechanisms of function. *Chem. Rev.* **96**, 601–617 (1996).
- Lowenstam, H. A. Minerals formed by organisms. *Science* **211**, 1126–1131 (1981).
- Addadi, L. & Weiner, S. Control and design principles in biological mineralization. *Angew. Chem. Int. Edn.* **31**, 153–169 (1992).
- Gref, R. *et al.* The controlled intravenous delivery of drugs using PEG-coated sterically stabilized nanospheres. *Adv. Drug Deliv. Rev.* **16**, 215–233 (1995).
- Panyam, J. & Labhasetwar, V. Biodegradable nanoparticles for drug and gene delivery to cells and tissue. *Adv. Drug Deliv. Rev.* **55**, 329–347 (2003).
- Kalsin, A. M., Kowalczyk, B., Smoukov, S. K., Klajn, R. & Grzybowski, B. A. Ionic-like behavior of oppositely charged nanoparticles. *J. Am. Chem. Soc.* **128**, 15046–15047 (2006).
- Kalsin, A. M., Kowalczyk, B., Wesson, P., Paszewski, M. & Grzybowski, B. A. Studying the thermodynamics of surface reactions on nanoparticles by electrostatic titrations. *J. Am. Chem. Soc.* **129**, 6664–6665 (2007).
- Kalsin, A. M. *et al.* Electrostatic self-assembly of binary nanoparticle crystals with a diamond-like lattice. *Science* **312**, 420–424 (2006).
- Kowalczyk, B. *et al.* Size selection during crystallization of oppositely charged nanoparticles. *Chem. Eur. J.* **15**, 2032–2035 (2009).
- Templeton, A. C., Zamborini, F. P., Wuelfing, W. P. & Murray, R. W. Controlled and reversible formation of nanoparticle aggregates and films using Cu²⁺-carboxylate chemistry. *Langmuir* **16**, 6682–6688 (2000).
- Wang, D., Tejerina, B., Lagzi, I., Kowalczyk, B. & Grzybowski, B. A. Bridging interactions and selective nanoparticle aggregation mediated by monovalent cations. *ACS Nano* **5**, 530–536 (2011).
- Tretiakov, K. V. *et al.* Mechanism of the cooperative adsorption of oppositely charged nanoparticles. *J. Phys. Chem. A* **113**, 3799–3803 (2009).
- Bishop, K. J. M., Wilmer, C. E., Soh, S. & Grzybowski, B. A. Nanoscale forces and their uses in self-assembly. *Small* **5**, 1600–1630 (2009).
- Smoukov, S. K., Bishop, K. J. M., Kowalczyk, B., Kalsin, A. M. & Grzybowski, B. A. Electrostatically ‘patchy’ coatings via cooperative adsorption of charged nanoparticles. *J. Am. Chem. Soc.* **129**, 15623–15630 (2007).
- Jones, F., Richmond, W. R. & Rohl, A. L. Molecular modeling of phosphonate molecules onto barium sulfate terraced surfaces. *J. Phys. Chem. B* **110**, 7414–7424 (2006).
- Kowalczyk, B., Lagzi, I. & Grzybowski, B. A. ‘Nanoarmoured’ droplets of different shapes formed by interfacial self-assembly and crosslinking of metal nanoparticles. *Nanoscale* **2**, 2366–2369 (2010).

Acknowledgements

This work was supported by the Non-equilibrium Energy Research Center, which is an Energy Frontier Research Center funded by the US Department of Energy, Office of Science, Office of Basic Energy Sciences under award number DE-SC0000989.

Author contributions

B.K. carried out the majority of experiments and imaging studies, and produced the figures; K.J.M.B. developed theoretical models; I.L. and D.W. helped with NP synthesis; Y.W. and S.H. collected and interpreted crystallographic data; B.A.G. conceived the project and wrote the paper.

Additional information

The authors declare no competing financial interests. Supplementary information accompanies this paper on www.nature.com/naturematerials. Reprints and permissions information is available online at <http://www.nature.com/reprints>. Correspondence and requests for materials should be addressed to B.A.G.

Charged nanoparticles as supramolecular surfactants for controlling the growth and stability of microcrystals

Bartłomiej Kowalczyk, Kyle J. M. Bishop, Istvan Lagzi, Dawei Wang, Yanhu Wei, Shuangbing Han and Bartosz A. Grzybowski

Nature Materials <http://dx.doi.org/10.1038/nmat3202> (2012); published online 10 January 2012; corrected online 20 January 2012.

In the version of this Letter originally published online, the name of the penultimate author was spelt incorrectly; it should have read Shuangbing Han. This error has been corrected in all versions of the Letter.